

ReaxFF Simulations of Self-Assembled Monolayers On Silver Surfaces and Nanocrystals

A. Lahouari,¹ J.-P. Piquemal,¹ J. Richardi^{1*}

1 Sorbonne Université, Laboratoire de Chimie Théorique, UMR 7616 CNRS, 75005 Paris, France. Email : Johannes.richardi@sorbonne-universite.fr

Abstract

The self-assembled monolayers of alkane thiolates on Ag (111) surfaces and nanoparticles are studied using molecular dynamics. Reactive force fields allow simulations of very large systems such as nanoparticles of 10 nm. Stable $(\sqrt{7} \times \sqrt{7})R19.1^\circ$ assemblies are obtained as experimentally observed for these systems. Only nanoparticles smaller than 4 nm show a spontaneous restructuration of the metallic core. The preferred adsorption site is found to be in an on-top position, in good agreement with recent X-ray absorption near edge structure experiments. Moreover, similar distances between the sulfur headgroups are found on the facets and edges.

1. Introduction

Silver nanoparticles (NPs) are characterized by unique optical, electrical, thermal and biological properties.^{1,2} In particular they are employed as antibacterial agents in tissues, food products and health care.³ Therefore, nano-silver is nowadays one of the most widely used nanomaterial. For many applications, silver NPs are protected by ligands such as thiolates or amines. These ligands form self-assembled monolayers (SAMs) on the NP surface. Alkane thiolates are for example used to tune the antibacterial properties of the silver NPs.³ Their presence modulates the Ag^+ ion release and helps to avoid non-desirable side effects. Recently the synthesis of atomically defined thiolate protected nano clusters was achieved opening up many possible applications.^{4,5}

Our study focuses on the alkane thiolates SAM which form on an Ag (111) surfaces and NPs. Experimentally a $(\sqrt{7} \times \sqrt{7})R19.1^\circ$ SAM (denoted as 77 SAM in the following) is observed.^{6,7} This contrasts to the Au (111) surfaces where $c(2 \times 4)$ and $(\sqrt{3} \times \sqrt{3})R30^\circ$ SAMs (denoted as 33) are seen. The former is usual caused by the formation of staples which corresponds to a restructuring of the surface.^{8,9} Experimental and theoretical studies have also shown that, due to the presence of thiolates, the silver surface can be restructured.^{6,7} In this case a silver atom appears between three sulfur atoms of the thiolates, due to bonds breaking on the surface. For this first study we focus however on non-restructured silver facets.

Silver NPs protected with thiolates have been widely studied by experiments in the last years¹⁰⁻¹⁶ using techniques like EXAFS (extended X-ray absorption fine structure), XANES (X-ray absorption near edge structure) or XPS (synchrotron-based X-ray photoelectron spectroscopy). These experiments led to two central questions. First, in some experiments the presence of silver sulfide was observed between the Ag core and the surrounding thiolates.^{10,11,16} However, other experiments found only a small amount of silver sulfide.¹²⁻¹⁶ The eventual origin of silver sulfides is not elucidated until now.¹⁶ Second, very recent experiments indicate an on-top adsorption site for the thiolates. This is in contradiction to recent theoretical Density Functional Theory (DFT) studies which predict a preference for the bridge position on flat silver surface and NPs.^{17,18}

The aim of this paper is to apply the recently developed ReaxFF¹⁹ force field (FF) in order to perform molecular dynamics simulations of thiolate SAMs on silver. Very recently several aspects of silver NPs have been studied using FF simulations²⁰⁻²⁴ and DFT calculations.¹⁸ In particular, the interaction between silver NPs and proteins²⁰ or amines²¹ and the formation of hollow silver NPs under laser irradiation.²²

However, to the best of our knowledge, there is only one study who focused on thiolates Ag (111) surfaces.²⁴ These simulations do not succeed to reproduce the 77 SAM on silver that were experimentally found. Moreover, no simulation of silver NPs with thiolates has been published. The use of ReaxFF may improve this situation for three reasons.

First, classical force fields using for example Lennard-Jones parameters naturally lead to hollow sites as preferred adsorption sites (see for example the study in reference 25). This is due to the fact that the hollow sites enable more contacts between the adsorbing atom and the metallic atoms. Therefore, such FFs have difficulties to simulate 77 SAMs characterized by the adsorption of bridge and on-top sites. Within the ReaxFF the Ag-S interaction is handled as a bond and angle dependent interactions enable to stabilize the adsorption of bridge and on-top sites compared to the hollow sites. Thus, we will show here that the new FF is able to reproduce the 77 SAM on Ag (111) planes in agreement with experiment.

Second, the silver surface may be restructured. This can only be simulated with reactive FFs allowing for the breaking of the Ag-Ag bonds: this would be the case for ReaxFF. Moreover, ReaxFF enables us to study if the thiolate is decomposed during adsorption which may explain the formation of silver sulfide.

Third, with the help of massively parallel computing, ReaxFF can investigate NPs made of hundred thousand of atoms in contrast to DFT methods. Thus, the largest system studied here is the butane thiolate coated NP of 10 nm made of 57826 atoms. Moreover, the evolution with temperature can also be studied which implies simulations lengths up to 4 ns. Such ReaxFF has been already applied for several metallic NPs made of cobalt, copper and gold.¹⁴⁻¹⁸ In particular for gold NPs, it predicts staple formation and on-top adsorption sites in full agreement with experiments.¹⁸

Here, the ReaxFF is used to calculate the properties of silver surfaces and NPs (with diameter from 2 to 10 nm) coated with thiolates. To study the influence of the chain length, methane and butane thiolates are used. While methane thiolates have been widely studied on flat silver surfaces, for NPs usually longer chains with at least butane have been used. For the sake of the comparison, we here nevertheless investigated also methane thiolate on NPs. In this first study we start from non-restructured surfaces to see if the restructuring spontaneously happens as previously observed for gold NPs with thiolates. We also ignore the presence of the solvent. It is expected that the solvent plays a minor role for the adsorption properties mainly governed by the strong Ag-S interactions. However, it might be non negligible for the energy difference between 77 and 33 SAMs which should be investigated in future.

The study focuses on nanocrystals of octahedral shape which has been chosen since their facets are made of Ag (111) planes. This enables a direct comparison with the results obtained for the Ag (111) surfaces. Moreover, NPs of octahedral shape are often observed in experiments.¹⁹

The structure of this paper is as follows. First, we will present the ReaxFF approach and the simulation protocols. We will then introduce the new analysis tools SAMmaker and SAMfinder that were specifically developed for this study. They allow to construct and find SAMs on metallic surfaces and NPs. Then the stability of the thiolate SAMs on Ag (111) surfaces is investigated. Finally, we will turn to the predicted properties of SAMs on NPs.

2. Method

2.1. The ReaxFF model

The reactive force field method proposed by van Duin et al.³² enables the formation and breaking of bonds during classical molecular dynamics simulations. The formalism is described in detail in the paper by Chemoweth et al.³³ Here, we use the recently developed FF for AgSCH.¹⁹ It is able to reproduce the DFT values for the average distances between silver atoms in NPs within a precision of 0.05 Å. It also correctly describes the energetical and geometric properties of thiolates on an Ag₂₀ pyramid arrangement.¹⁹

The charges of the atoms are obtained through the usual electronegativity equalization method (EEM).^{34,35}

2.2 Simulation protocol

Molecular dynamics simulations are carried out in the NVT ensemble using a timestep of 0.25 fs. The temperature is controlled using the Berendsen thermostat with a damping constant of 5 fs. The parallel program LAMMPS is used for all simulations.^{36,37} First, an equilibration is performed increasing the temperature from 0 to 300 K. The simulation is then continued at 300 K to obtain better converged properties. To test correct equilibration and convergence three runs are performed:

- Equilibration: 0.3 ns, convergence at 300 K: 0.3 ns
- Equilibration: 1 ns, convergence at 300 K: 1 ns
- Equilibration: 3 ns, convergence at 300 K: 1 ns

To obtain standard errors for all properties three independent simulations are carried out starting from different initial atomic positions for the SAM position with a shift of 0.05 Å.

2.3 Set up tools

A new python tool called SAMmaker was developed to set up SAMs on flat surfaces and NPs. It has been included in the python library NATOMOS. How this tool is working is explained in the supporting information.

We observed that it is very important to have a compact initial layer of alkane without strong repulsion to obtain stable SAMs. Therefore, all ligands are slightly declined and oriented in the same directions. Moreover, orientations with very small repulsions were searched for. Figure 1 shows typical snapshots obtained after equilibration for a 77 and 33 SAM of thiolates on Ag (111) surface.

To set up the NPs, the SAMs obtained with SAMmaker are transferred on the NP facets using the NATOMOS tool NTM_setup which has been described in detail in a previous paper.³⁰ It is interesting to note that there are differences in the stability of SAMs for NPs compared to surfaces. Thus, starting from an orientation of the methane thiolate with S-C bond perpendicular to the plane lead to a well-defined SAM on the surface. However, when the same orientation is used for NPs, the SAM becomes unstable during the simulation. This shows the importance to well define the initial orientation to obtain a large degree of SAMs.

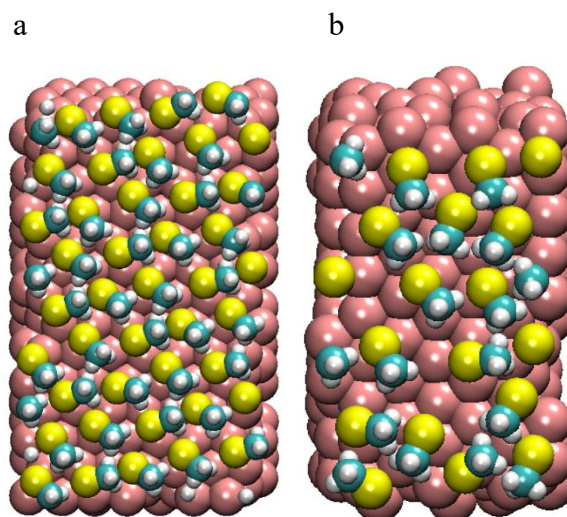


Figure 1: Snapshots of a SAM of methane thiolates on Ag(111) at 300 K after an equilibration of 0.3 ns. (a) 77 SAM, (b) 33 SAM.

2.4 Analysis tools

The SAMs were analyzed with the help of the python tool NTM_ana. It was described in detail in a previous paper.³⁰ It determines the following properties studied in this paper:

- the number of neighbors for the silver atoms,
- the locations and types of the adsorption sites occupied by the ligands,
- the average distances of neighboring ligand head groups.

Please note that two atoms are counted as neighbors whenever the distance is smaller than the position of the minimum after the first peak of the pair distribution function (minimum for Ag-Ag: 3.75 Å, Ag-S: 2.92 Å and S-S: 5.5 Å)

Here a new function SAMfinder has been included in Ntm_ana. It allows to determine the percentage of ligands participating in a SAM characterized as 33 or 77, for example. For this purpose, a percolation method is used which is explained in detail in the SI. All properties obtained by the analysis are shown in table S1 to S4 in the SI.

3. Thiolate SAMs on Ag(111) surfaces

Simulations on two different thiolate SAMs on an Ag (111) plane were carried out (see figure 1). On one hand, the 77 SAM experimentally observed on non-restructured Ag(111) surfaces is studied. On the other hand, we also investigated the 33 SAM for silver usually observed on an Au (111) when no staple formation occurs. The second SAM was chosen for the following reason. The Ag (111) and Au (111) surfaces have the same geometry leading to the same distances between the ligands in a given SAM. Moreover, staple formation such as for Au (111) is not observed on Ag (111). Therefore, the 33 SAM without staples should also be possible for steric reasons on Ag (111). A successful forcefield should however predict that the 77 SAM is more stable than the 33 SAM in agreement with experiments.

We now study the simulations starting from a 77 and 33 SAMs as a function of the temperature. Figure 1 shows snapshots of both SAMs obtained at 300 K. First the stability of the SAMs during the simulation is studied. Then, their energies and entropies are compared and finally their properties such as the occupation of adsorption sites are discussed.

3.1. Stability of the SAMs on silver surfaces

Figure 2 plots the percentage of thiolates belonging to a 77 and 33 SAM for methane and butane thiolate obtained for the longest simulation run (3 ns) as determined with the module SAMfinder. The results for both 77 and 33 SAMs at different simulation times are shown in the SI (Figure S11).

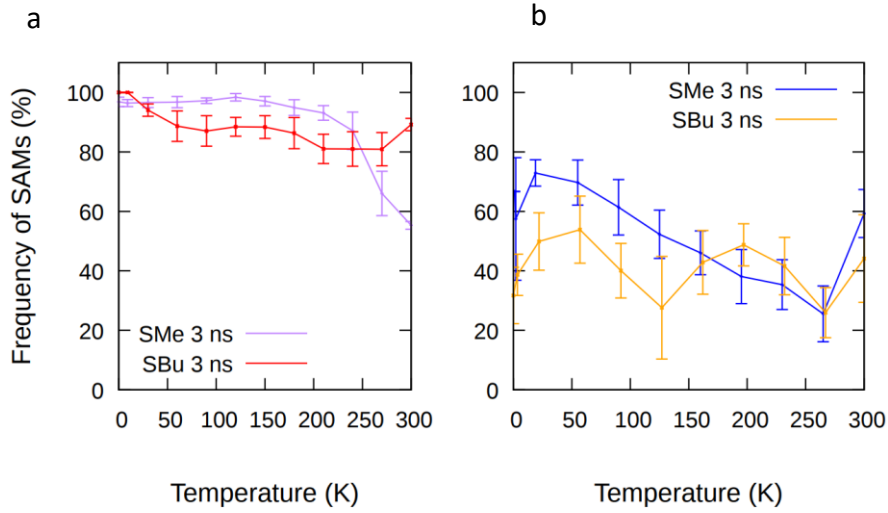


Figure 2: Frequencies of 77 (a) and 33 (b) SAMs of methane and butane thiolates on Ag (111) surface for an equilibration step of 3 ns corresponding to an increase of the temperature.

In the case of butane thiolate, the 77 SAM occupied nearly the total surface up to 300 K independent on the simulation time. This is also found for methane thiolate until 250 K. However, at higher temperature the percentage of methane thiolates in 77 SAMs decreases. This becomes more pronounced when the simulation time used for the equilibrations increases (see Figure SI1). To investigate the stability of the 77 SAM at 300K the simulation run is continued for 1 ns at that temperature (see Figure SI2). We observed a completely disappearance of the 77 SAM for methane thiolate in contrast to butane thiolate which rests stable. Studying the snapshots at 300 K (see Figure SI3), we found a desorption of the methane thiolates which is not observed in experiments. Thus, it shows the limit of our forcefield. Since we want to study stable SAMs, we only considered simulations before this happens (the first 10000 steps at 300 K). Figure 2 shows also the frequency of 33 SAMs starting from a perfect 33 SAM where the frequency of SAM rapidly decreases to about 20% for the methane and stay stable for the butane with some fluctuation during the simulation.

3.2. Energy and entropy of the SAMs

In order to compare the stability of both SAMs, we first calculate their binding energies per thiolates defined as:

$$\Delta E_{bind} = \frac{1}{n_{Thio}} (E^{M-SAM} - E^{Metal} - n_{Thio} E^{Thiolate})$$

where E^{M-SAM} corresponds to the energy of the system which corresponds to the SAMs in contact with the metal layer. E^{Metal} and $E^{Thiolate}$ are respectively the energies of the metal layer and of the single thiolate molecule. n_{Thio} corresponds to the number of thiolates present on the surface. By calculating the difference between the ΔE_{bind} of the 77 and the 33 SAMs

one can easily see that the calculation of $E^{Thiolate}$ is not necessary which allows us to decrease the possible errors that can emerge with the simulation of small system using ReaxFF.

Figure 3 displays the evolution of the binding energies as a function of the temperature for methane and butane thiolates on silver for 3 ns. In Figure SI4 the results for 0.3 and 1 ns are shown. It is obvious that sufficiently long simulation runs have to be carried out to obtain stable results.

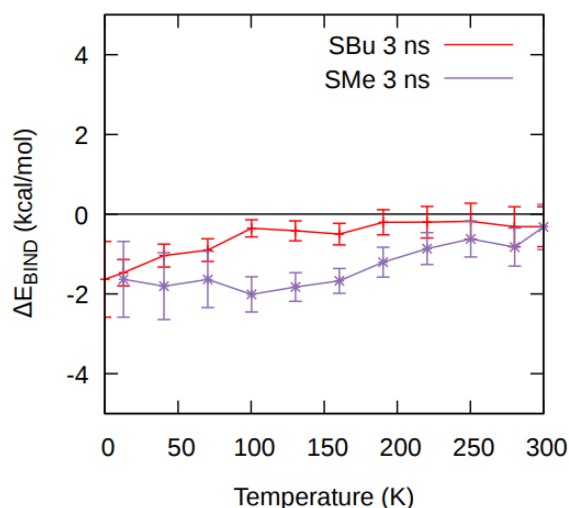


Figure 3: Difference of binding energies between the 77 and the 33 SAMs as a function of the temperature for both butane and methane thiolates on the Ag(111) surface. Simulation length: 3 ns.

In the case of methane thiolate, Figure 3 shows that the binding energy difference varies between -2 and -1 kcal.mol⁻¹. This indicates that the 77 SAM is energetically favored. However, for the butane thiolate, the binding energy difference is between -2 and 0 kcal.mol⁻¹. Hence, the energetical stabilization of the 77 conformation is not proved in this case.

In order to know which SAM is the most stable one, we need to consider the influence of entropy. It can be estimated from statistical mechanics using the partition function of translation. The ligand molecule can move within the space left by the neighboring ligands. For the 33 SAM this space is larger due to a larger surface per thiolate than for the 77 SAM. It is therefore expected that the 33 SAM is entropically favored. The evaluation of the free energy part due to entropy is carried out in the SI and at 300 K gave 0.149 kcal.mol⁻¹ between the 77 and the 33 SAM. This shows that the entropy favors 33 SAMs as expected. However, in the case of methane thiolate, the binding energy is much larger than the estimated free energy due to entropy. This means that the 77 SAM is the more stable assembly for our force field in good

agreement with experiment. As discussed above this conclusion cannot be made in the case of butane thiolate.

3.3. The properties of the 77 SAMs

We now look at the properties of the 77 SAMs which will be important for the comparison with the results obtained in the following section for the NPs. For methane thiolate, we calculate properties after the first 10 000 steps at 300 K to avoid the part of simulation where the desorption of the ligands starts.

It is important to note that during all simulations no spontaneous decomposition of the ligands is observed. We first study the number of Ag neighbors around a silver atom. The expected numbers of 12 and 9 neighbors for the bulk and surface atoms, respectively were obtained as shown in Figure SI5. No spontaneous restructuring of the metallic layer is observed. DFT theory and experiments however have shown such a restructuring.^{6,7} This may mean that such a restructuring is too slow to take place in our simulations. In future simulations starting from a restructured surface are planned to study their stability and properties in comparison with the non-restructured layer investigated here.

We now turn to the occupation frequencies of adsorption sites shown in Figure SI6 for butane and methane thiolates. A comparison of the results obtained after 1 and 3 ns shows an agreement within the statistical accuracy which indicates that the results are well converged. A similar occupation of the on-top (52 %) and bridge (48 %) sites is found where the S atom is in contact with one and two silver atoms, respectively. These sites are typically occupied in 77 SAMs when studied by DFT.⁶ Please note that we found that these sites are usually occupied in a way, so that the adsorbing atom is shifted from the ideal on-top or bridge site.

Finally, the average distance between the sulfur head groups of the ligands was determined (Figure SI7). A value of 4.4 Å is found which corresponds to the one expected for the 77 SAM.

4. Thiolate SAMs on silver Nanoparticles

Figure 4 shows the typical snapshot obtained for a simulation of 2 and 10 nm NP with butane thiolate at 300 K (1 ns). Figure SI8 presents snapshots for 4 nm. The NPs of 2 and 4 nm are also shown without the ligands to make any restructuring visible. No spontaneous decomposition of the thiolates was observed. Therefore, the formation of silver sulfide observed in some experiments^{10,11,16} cannot be explained by these experiments. However, we cannot exclude that a restructured silver layer may lead to this kind of decomposition, which should

be studied in future. Also, other ligands such as allyl thiolate (for which silver sulfide has been often observed^{11,16}) should be tested. We will now first study if the 77 SAM is also stable on NPs. In the following, the properties such as the occupation of adsorption sites and the distance between the sulfur atoms is discussed for the NPs.

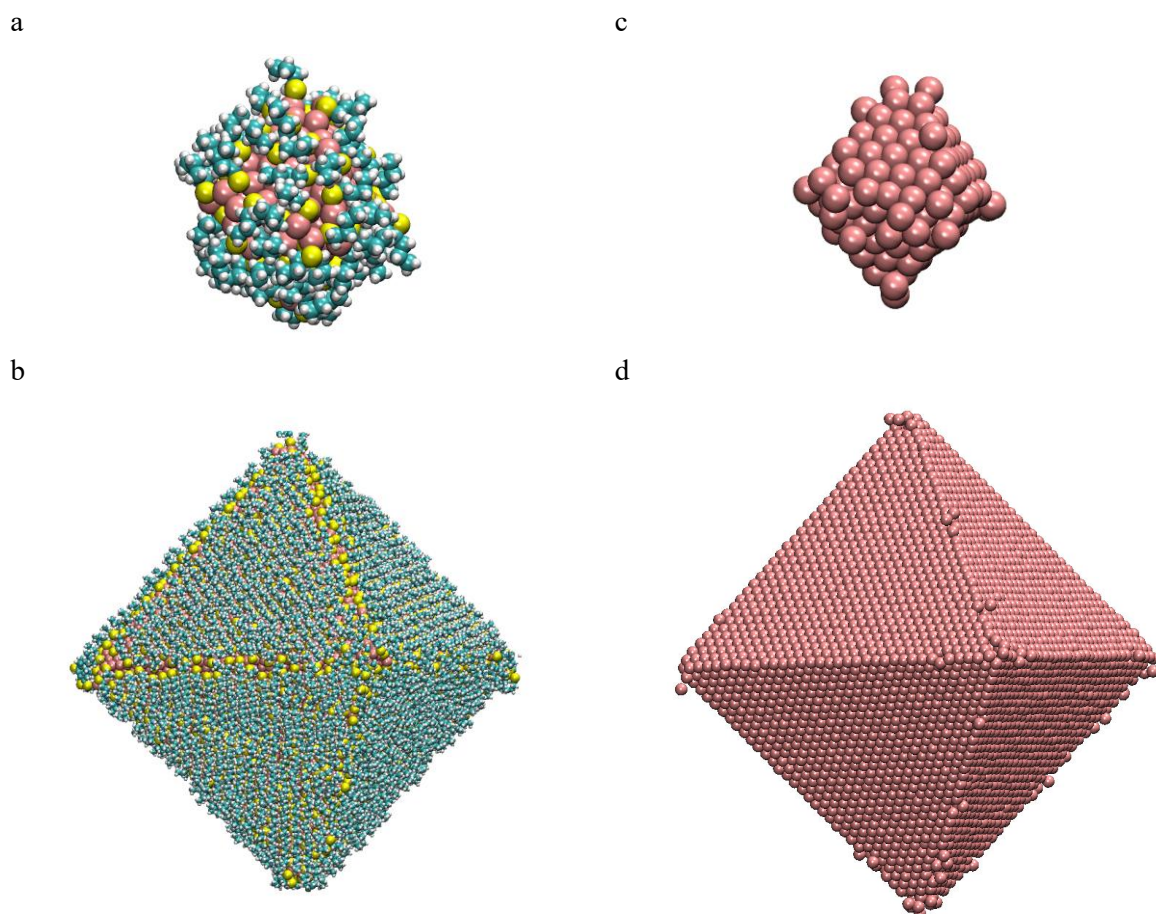


Figure 4: Snapshots of the simulation of butane thiolate covered silver nanoparticles of 2 nm (a) and 10 nm (b) at the end of the convergence step for 1 ns at 300 K. The ligands are removed to show any reconstruction of the metallic core on c and d snapshots.

4.1. Is the 77 SAM stable on nanoparticles?

We now study the frequency at which 77 SAMs are found on the NPs for both ligands (Figure 5: for 3 ns, Figure SI9: for 0.3, 1 and 3 ns and NP size of 4 nm). We first focus on 4 nm NP to evaluate the convergence of the simulation results in Figure SI9.

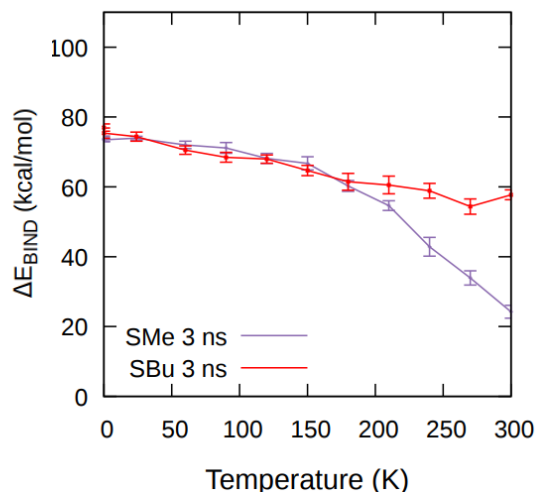


Figure 5: Frequencies of 77 SAMs on a 4 nm Ag (111) NP for methane and butane thiolates depending on the temperature. Equilibration time of 3 ns.

For both ligands the same frequency around 70% is found at low temperatures. This is significantly lower than the frequencies between 90 and 100% observed on the flat surfaces (see figure 2). To understand this difference, we study where the SAMs are located (Figure SI10). Therefore, all atoms belonging to SAMs are colored as red. They are found principally in the centers of the facets and the SAMs formation is perturbed by the edges. By increasing the temperature, the SAM frequency decreases.

For butane thiolate a 77 SAMs frequency of 60% is observed at 300 K. In the case of methane thiolate, a more pronounced decrease is found from 200 K as observed on the flat surface. This decrease depends on the length of simulations as for the surface (see Figure SI9), but even after an additional run of 1 ns the frequency in SAMs stays stable at 20%.

Now let us look at the evolution of the 77 SAM frequency with the particle size (see figure 6). From 2 to 10 nm the SAMs frequency decreases at 300 K for butane thiolate. Nevertheless, depending on the NP diameter, the decrease is more or less pronounced. The more we increase the NP diameter the more the coverage of the facets grows and the SAM formation is then less perturbed by the edges. This is the reason why we have a 20% decrease for 2 and 4 nm and a 5% decrease for NPs from 6 to 10 nm. For the methane thiolates we can see that we have a large decrease of about 30% as found from previous result on the surface, moreover it can be seen that it does not depend on the size of the NP.

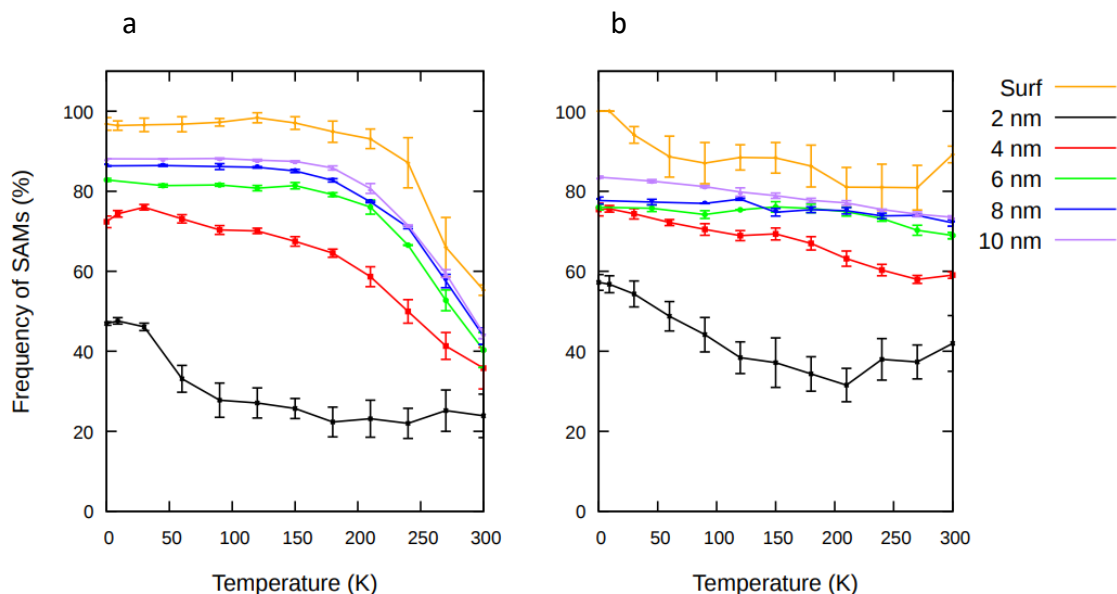


Figure 6: Frequencies of 77 SAMs on NPs for methane (a) and butane (b) thiolates depending on the temperature. Comparison between surfaces and NPs of different sizes from 2 to 10 nm; equilibration time of 1 ns.

4.2. The structure of the metallic core

We now turn to the number of neighbors observed for the silver atoms. For a perfect octahedron 7 and 9 neighbors are found on the edges and facets, respectively. A change in these numbers would indicate a surface restructuring due to the ligands. Such a phenomenon was widely observed in the ReaxFF simulation for gold NPs, where the metallic atoms were extracted on the facets and, in particular, at the edges due to staple formation.^{29,30} Figure 7 shows the frequencies of silver atoms as a function of their number of neighbors for different NP size with butane thiolate SAMs. In the SI (Figure SI11) the neighbor frequencies of 4 nm NPs are plotted for both ligands and different simulation times. This figure shows that the results for both thiolates are very similar. The frequencies of neighbors also agree for the three runs of different length showing that these results are well converged.

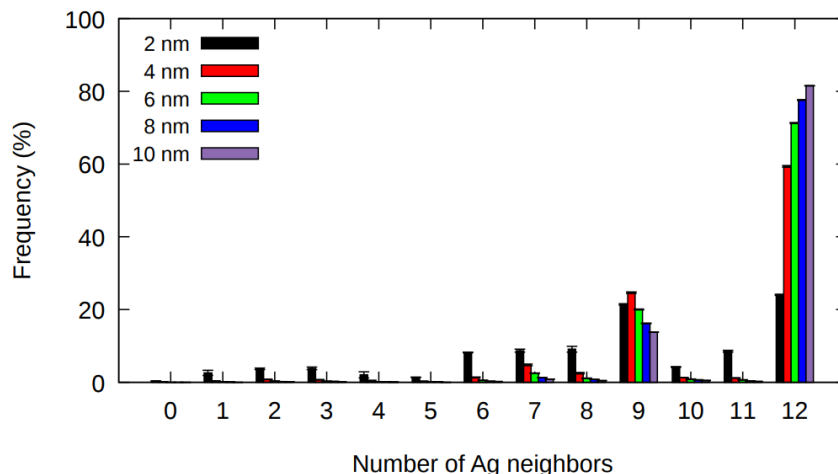


Figure 7: Frequencies of silver atoms as a function of the number of neighbors for NPs from 2 to 10 nm for butane thiolate (equilibration time of 1 ns and convergence time of 1 ns). Property taken at the end of the convergence at 300K.

By focusing on Figure 7 it can be seen that the neighbor frequencies for the NPs larger than 2 nm are similar to a perfect octahedron with peaks for 7, 9 and 12 neighbors. Only at the edges some atoms change their positions leading to atoms with 6 or 8 neighbors. These results are very different from the ones found for gold NPs previously discussed.³⁰ This shows that no surface restructuration spontaneously happens for large silver NPs.

However, for the 2 nm NP the behavior is markedly different (see black lines in Figure 6). A large fraction of atoms changes the number of neighbors even on the facets. This change in morphology is confirmed in the snapshots shown in the SI (Figure SI8).

4.3 Location and occupation of adsorption sites

We will first see where the ligands are located on the NP surface. Ligands are counted for the vertices or edges if they are in contact with at least one silver atoms on the vertices or edges, respectively. The remaining ligands are attributed to the facets. For example, in the case of 4 nm particles with butane thiolate 55.7%, 39.4% and 4.9% of the ligands are adsorbed on the facets, edges and vertices, respectively. These frequencies do not significantly change during the simulation and correspond to the ones initially set up. Similar behavior was observed for all NP size and ligands. In table SI2 all frequencies giving the location of ligands are collected.

We now turn to the question which adsorption sites the ligands occupy. In Figure 8 the frequencies of head groups as a function of their number of silver neighbors are shown for

butane thiolate and different NP sizes. On a perfect Ag (111) surface the head group of a ligand occupying the on-top, bridge or hollow site have 1, 2 or 3 neighbors, respectively. For NPs larger than 4 nm, this is also true here since the degree of silver atoms extracted by ligands is very low as previously shown and the NP surface is well described by the Ag (111) plane. The frequencies of neighbors agree for the three runs with different simulation lengths (see Figure SI12).

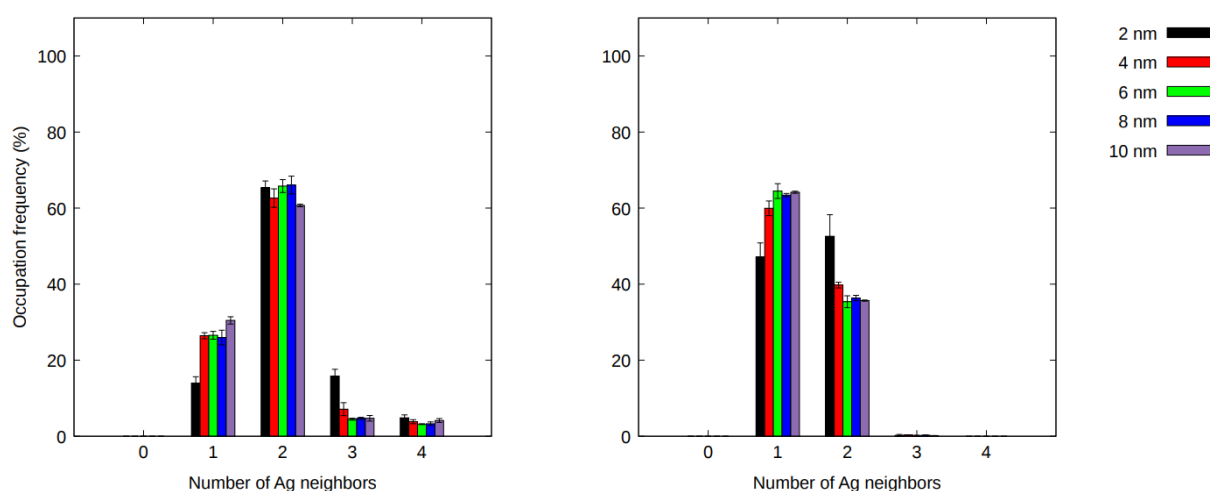


Figure 8: Occupation frequencies of S atoms in contact with a given number of silver atoms on the (a) edges and (b) facets for butane thiolates on Ag (111) nanostructure from 2 to 10 nm with a simulation length of 1 ns at the end of the convergence at 300 K.

Similar to the surface results discussed in Section 3.1., the ligands on the NP facets occupy only on-top and bridge sites with a preference of the on-top site. The results do not depend on the length of the alkane chain as shown in Figure SI12. Also, the NP size has little influence on the occupation frequencies except for the smallest NP of 2 nm. On the NPs edges, the results are quite different where the head groups are mainly in contact with two atoms which indicates a preference of the bridge site.

The occupation of the on-top sites found on the facets and edges are in good agreement with recent S-edge XANES experiments,¹⁶ which clearly show an occupation of this site. Here we show that this occupation is related to a dense assembly such as the 77 SAM, which can only be realized by occupying both on-top and bridge sites. This explains the occupation of the on-top sites even when the bridge sites are preferred as shown in DFT calculations.^{17,18} In contrast, less dense assemblies such as the 33 SAM would imply only an occupation of the bridge site not consistent with experiments.

In the gold NPs ReaxFF simulations, an on-top site preference has also been observed on the facets. This appears to be in good agreement with experiments.³⁰ In contrast the

observation here that the head groups are only bonded to one or two atoms is very different from the simulations of gold NPs where a large fraction of ligands was also in contact with three or even four gold atoms.

Finally, we study the average distances between neighboring sulfur head groups of the ligands. The S-S distances are shown in Figure 9 for butane thiolate and different NP sizes. The corresponding results for methane thiolate shown in the SI (Figure SI13) is very close and does not depend on the length of simulation. The S-S distance is close to 4.4 Å for both the edge and the facet as expected for a 77 SAM. For NPs larger than 4 nm, this distance does not evolve with the NP size or alkane chain length of the ligand. There is also no significant difference between the edge and the facet. In a previous simulation of gold NPs using non-reactive force fields,^{37,38} the S-S distances on the edges were found about 0.2 Å smaller than those on the facets which implies a different assembly on the edges. These results could not be confirmed by recent ReaxFF simulations for gold NPs. Here, we show that also for silver the S-S distance on the edges is not reduced. For smaller NPs of 2 nm, the average S-S distance increases to 4.5 nm and the distances on the edges is slightly reduced with respect to the facets.

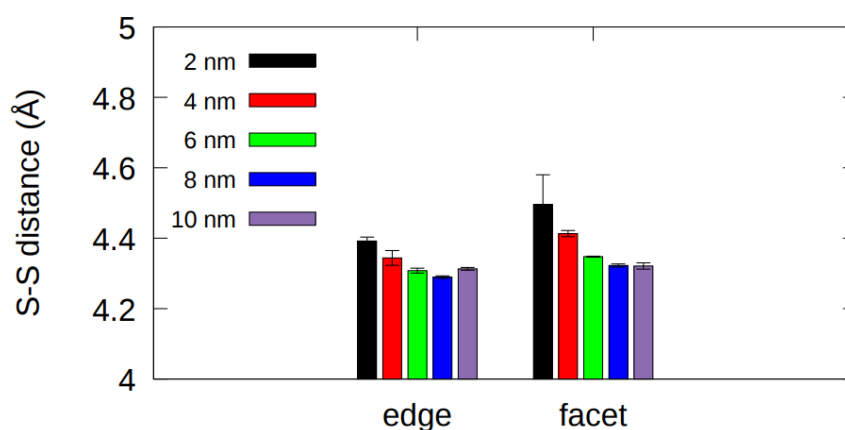


Figure 9: Average S-S distance between first neighbors on the edges and facets of silver NPs from 2 to 10 nm for butane thiolates at the end of convergence at 300K for an equilibration length of 1 ns.

Conclusion

We have shown here that the ReaxFF approach is able to reproduce the 77 SAM typical of alkane thiolates on the Ag (111) surface. In a recent paper, it was also shown that ReaxFF was capable to reproduce the formation of staples on Au (111) surfaces. Thus, it is possible with ReaxFF to distinguish both materials which is usually quite difficult for FFs, since both metals are characterized by the same geometry. However, we observed that the 77 SAM of methane

thiolate is not stable for very long simulations. In addition, the SAM for butane thiolate is not energetically favored with respect to other SAMs. This shows the model current parametrization limits.

The simulations here also show that dense assemblies like those found on the 77 SAM should appear on silver NPs. To the best of our knowledge, there are no available experiment studying this question. During the simulations no decomposition of the alkane thiolate are found which could explain the formation of silver sulfide observed in some experiments.^{10,11,16} In the future, this question should also be investigated for restructured surfaces and other ligands.

Also, no spontaneous restructuring of the NP surfaces was found except for the small NPs inferior to 4 nm. This might be due to the fact that such a restructuring is a very slow process not attainable in our simulations. We plan to perform simulations starting from a restructured surface and compare its stability with those found here.

Two adsorption sites on silver NP facets were found : one on-top and another one at the bridge site where the former is preferred: this is in good agreement with recent experiments.

Regarding the distance between S-head group ligands, we observed no difference between the facets and the edges.

Supporting Information

This information is available free of charge via the Internet at <http://pubs.acs.org>

Section to discuss details of the paper; Figure 1 Ag (111) layer with the initial positions of the sulfur atoms in a 77 SAMs of thiolates. FILE “SIxtartncsilver” (PDF)

Table S1, average distances between neighboring S head groups for silver nanocrystals for both methane and butane; Table S2 relative frequencies of the S head group as a function of their adsorption position for silver nanocrystals for both methane and butane thiolate; Table S3 frequencies of silver atoms with a given number of neighbors for silver nanocrystals for both methane and butane thiolate; Table S4 frequencies of the S atoms in contact with a given number of silver atoms for silver nanocrystals for both methane and butane thiolate; FILE “SIxtartncsilver” (PDF)

Figure S1 Frequencies of 77 and 33 SAMs of methane and butane thiolates on Ag(111) surface for an equilibration of 0.3 and 1 ns; Figure S2 Frequencies of 77 SAMs of methane and butane thiolates on Ag (111) surface continuing the run after the equilibration of 3 ns for 1 ns; Figure S3 Snapshot of both the methane and butane thiolates SAMs on Ag(111) surface after 4 ns; Figure S4 Difference of binding energies between the 77 and the 33 SAMs as a function of the temperature for both butane and methane thiolates on the Ag (111) surface;

Figure S5 frequencies of atoms as a function of the number of Ag neighbours for an Ag (111) surface with a SAM composed of methane or butane thiolates at different simulation length from 0.3 ns to 3 ns; Figure S6 Occupation frequencies of adsorption sites on the facet for both methane and butane thiolates on Ag (111) surface; Figure S7 Average distance between sulfure atoms neighbours of methane and butane thiolates on a 77 SAM at different simulation lengths 1 ns and 3 ns; Figure S8 : Snapshots of the simulation of methane thiolate covered silver nanoparticles of 2 nm and 4 nm at the end of the convergence step for 1 ns at 300 K; Frequencies of 77 SAM for both methane and butane thiolates SAMs on a 4 nm Ag (111) NP for different for 0.3 ns, 1 ns and 3 ns simulation length during the equilibration step; Figure S10 Snapshots of the simulation of a 77 butane thiolate SAMs on Ag (111) nanoparticles of 4 nm at the end of the convergence step for 1 ns at 300 K; Figure S11 Frequencies of silver atoms as a function of their number of neighbours for 4 nm for methane and butane thiolate at different equilibration times from 0.3 ns to 3 ns; Figure S12 Occupation frequencies of adsorption sites on the edges and facets for both methane and butane thiolates on an Ag (111) nanoparticle of 4 nm, where respectively 1, 2 and 3 Ag neighbours correspond to top, bridge and hollow site; FILE “Sifigartncsilver”

Program for setup of surface conformation; FILE “SAM_maker.py” (TXT)

Program for setup of nanocrystal conformation; FILE “ntm_setup.py” (TXT)

Program for analysis of nanocrystal and surface simulations; FILE “ntm_ana.py” (TXT)

User guide for the programs; FILE “readme.txt” (PDF)

Methane_Thiolate_RightShift.xyz (XYZ)

Methane_Thiolates_straight.xyz (XYZ)

Butane_Thiolate.xyz (XYZ)

nc6octa.xyz (XYZ)

Methane_Thiolate.xyz (XYZ)

simu_ns6_SMe.xyz (XYZ)

ns6Ag287_77N.xyz (XYZ)

Author information

Corresponding Author

E-mail johannes.richardi@sorbonne-universite.fr (J.R.)

Notes

The authors declare no competing financial interest.

Acknowledgements. This work was granted access to the HPC resources of CINES/IDRIS/TGCC under the allocation 2021-A0080811426 (Responsible: J. Richardi) made by GENCI.

References

1. Morones, J. R.; Elechiguerra, J. L.; Camacho, A.; Holt, K.; Kouri, J. B.; Ramirez, J. T.; Yacaman, M.J. The bactericidal effect of silver Nanoparticles, *Nanotechnology* 2005, 16, 2346–2353.
2. Jain, P. K.; Huang, X.; El-Sayed, I. H.; El-Sayed, M. A. Noble Metals on the Nanoscale: Optical and Photothermal Properties and Some Applications in Imaging, Sensing, Biology, and Medicine, *Acc. Chem. Res.* 2008, 41, 1578-1586.
3. Le Ouay, B.; Stellacci, F. Antibacterial Activity of Silver Nanoparticles: A Surface Science Insight. *Nano Today* 2015, 10, 339– 354.
4. Alhilaly, M. J.; Bootharaju, M. S.; Joshi, C. P.; Besong, T. M.; Emwas, A.-H.; Juarez-Mosqueda, R.; Kaappa, S.; Malola, S.; Adil, K.; Shkurenko, A.; Häkkinen, H.; Eddaoudi, M.; Bakr, O. M. [Ag₆₇ (SPhMe₂)₃₂ (PPh₃)₈]³⁺: Synthesis, Total Structure, and Optical Properties of a Large Box-Shaped Silver Nanocluster. *J. Am. Chem. Soc.* 2016, 138 (44), 14727–14732.
5. Yang, H.; Wang, Y.; Huang, H.; Gell, L.; Lehtovaara, L.; Malola, S.; Häkkinen, H.; Zheng, N. All-Thiol-Stabilized Ag₄₄ and Au₁₂Ag₃₂ Nanoparticles with Single-Crystal Structures. *Nat. Commun.* 2013, 4 (1), 2422.
6. Torres, D.; Carro, P.; Salvarezza, R. C.; Illas, F. Evidence for the Formation of Different Energetically Similar Atomic Structures in Ag (111) – (7 × 7)–R 19.1 ° – CH₃ S. *Phys. Rev. Lett.* 2006, 97 (22), 226103.
7. Woodruff, D. P. The interface structure of n-alkylthiolate self-assembled monolayers on coinage metal surfaces. *Phys. Chem. Chem. Phys.* 2008, 10, 7211-7221.
8. Grönbeck, H.; Häkkinen, H.; Whetten, R. L. Gold-thiolate complexes form a unique c(4 × 2) structure on Au(111). *J. Phys. Chem. C* 2008, 112, 15940–15942.
9. Voznyy, O.; Dubowski, J. J.; Yates, J. T.; Maksymovych, P. The Role of Gold Adatoms and Stereochemistry in Self-Assembly of Methylthiolate on Au(111). *J. Am. Chem. Soc.* 2009, 131 (36), 12989–12993.

10. Padmos, J. D.; Zhang, P. Surface Structure of Organosulfur Stabilized Silver Nanoparticles Studied with X-Ray Absorption Spectroscopy. *The Journal of Physical Chemistry C* **2012**, *116* (43), 23094–23101. <https://doi.org/10.1021/jp3075332>.
11. Battocchio, C.; Meneghini, C.; Fratoddi, I.; Venditti, I.; Russo, M. V.; Aquilanti, G.; Maurizio, C.; Bondino, F.; Matassa, R.; Rossi, M.; Mobilio, S.; Polzonetti, G. Silver Nanoparticles Stabilized with Thiols: A Close Look at the Local Chemistry and Chemical Structure. *The Journal of Physical Chemistry C* **2012**, *116* (36), 19571–19578. <https://doi.org/10.1021/jp305748a>.
12. Farrag, M.; Thämer, M.; Tschurl, M.; Bürgi, T.; Heiz, U. Preparation and Spectroscopic Properties of Monolayer-Protected Silver Nanoclusters. *The Journal of Physical Chemistry C* **2012**, *116* (14), 8034–8043. <https://doi.org/10.1021/jp210453v>.
13. Maya Girón, J. V.; Zelaya, E.; Rubert, A.; Benítez, G.; Carro, P.; Salvarezza, R. C.; Vela, M. E. Surface Chemistry of 4-Mercaptobenzoic Acid Self-Assembled on Ag(111) and Ag Nanoparticles. *The Journal of Physical Chemistry C* **2013**, *117* (47), 24967–24974. <https://doi.org/10.1021/jp409785c>
14. Azcárate, J. C.; Corthey, G.; Pensa, E.; Vericat, C.; Fonticelli, M. H.; Salvarezza, R. C.; Carro, P. Understanding the Surface Chemistry of Thiolate-Protected Metallic Nanoparticles. *The Journal of Physical Chemistry Letters* **2013**, *4* (18), 3127–3138. <https://doi.org/10.1021/jz401526y>.
15. Vericat, C.; Vela, M. E.; Corthey, G.; Pensa, E.; Cortés, E.; Fonticelli, M. H.; Ibañez, F.; Benitez, G. E.; Carro, P.; Salvarezza, R. C. Self-Assembled Monolayers of Thiolates on Metals: A Review Article on Sulfur-Metal Chemistry and Surface Structures. *RSC Adv.* **2014**, *4* (53), 27730–27754. <https://doi.org/10.1039/c4ra04659e>.
16. Marchioni, M.; Battocchio, C.; Joly, Y.; Gateau, C.; Nappini, S.; Pis, I.; Delangle, P.; Michaud-Soret, I.; Deniaud, A.; Veronesi, G. Thiolate-Capped Silver Nanoparticles: Discerning Direct Grafting from Sulfidation at the Metal–Ligand Interface by Interrogating the Sulfur Atom. *The Journal of Physical Chemistry C* **2020**, *124* (24), 13467–13478. <https://doi.org/10.1021/acs.jpcc.0c03388>.
17. Li, A.; Piquemal, J. P.; Richardi, J.; Calatayud, M. Butanethiol adsorption and dissociation on Ag (111): A periodic DFT study. *Surf. Sci.* **2016**, *646*, 247–252.
18. Becerril, D.; Noguez, C. Adsorption of a Methylthio Radical on Silver Nanoparticles: Size Dependence. *The Journal of Physical Chemistry C* **2014**, *119* (20), 10824–10835. <https://doi.org/10.1021/jp509727q>.

19. Dulong, C.; Madebene, B.; Monti, S.; Richardi, J. Optimization of a New Reactive Force Field for Silver-Based Materials. *J. Chem. Theory Comput.* 2020, 16 (11), 7089–7099.
20. Hazarika, Z.; Jha, A. N. Computational Analysis of the Silver Nanoparticle–Human Serum Albumin Complex. *ACS Omega* 2019, 5 (1), 170–178.
<https://doi.org/10.1021/acsomega.9b02340>.
21. Yoneya, M.; Sugisawa, S. Simulation of Colloidal Silver Nanoparticle Formation from a Precursor Complex. *The Journal of Physical Chemistry C* 2019, 123 (17), 11257–11263. <https://doi.org/10.1021/acs.jpcc.9b01360>.
22. Jiang, C.; Mo, Y.; Wang, H.; Li, R.; Huang, M.; Jiang, S. Molecular Dynamics Simulation of the Production of Hollow Silver Nanoparticles under Ultrafast Laser Irradiation. *Computational Materials Science* 2021, 196, 110545.
<https://doi.org/10.1016/j.commatsci.2021.110545>.
23. Gu, M.; Liu, T.; Xiao, X.; Li, G.; Liao, W. Simulation and Experimental Study of the Multisized Silver Nanoparticles Sintering Process Based on Molecular Dynamics. *Nanomaterials* 2022, 12 (6), 1030. <https://doi.org/10.3390/nano12061030>.
24. Alexiadis, O.; Harmandaris, V. A.; Mavrantzas, V. G.; Delle Site, L. Atomistic Simulation of Alkanethiolate Self-Assembled Monolayers on Different Metal Surfaces via a Quantum, First-Principles Parametrization of the Sulfur-Metal Interaction. *J. Phys. Chem. C* 2007, 111, 6380–6391.
25. Djebaili, T.; Abel, S.; Marchi, M.; Richardi, J. Influence of Force-Field Parameters on the Atomistic Simulations of Metallic Surfaces and Nanoparticles, *J. Phys. Chem. C* 2017, 121, 27758–27765.
26. Zhang, X.-Q.; Iype, E.; Nedeia, S. V.; Jansen, A. P. J.; Szyja, B. M.; Hensen, E. J. M.; van Santen, R. A. Site Stability on Cobalt Nanoparticles: A Molecular Dynamics ReaxFF Reactive Force Field Study, *J. Phys. Chem. C* 2014, 118, 6882–6886
27. Keith, J. A.; Fantauzzi, D.; Jacob, T.; Van Duin, A. C. Reactive forcefield for simulating gold surfaces and nanoparticles. *Phys. Rev. B* 2010, 81, 235404.
28. Bae, G.-T.; Aikens, C. M. Improved ReaxFF Force Field Parameters for Au–S–C–H Systems. *J. Phys. Chem. A* 2013, 117 (40), 10438–10446.
<https://doi.org/10.1021/jp405992m>.
29. Monti, S.; Carravetta, V.; Ågren, H. Simulation of Gold Functionalization with Cysteine by Reactive Molecular Dynamics. *J. Phys. Chem. Lett.* 2016, 7 (2), 272–276.
<https://doi.org/10.1021/acs.jpcclett.5b02769>.

30. Richardi, J.; Fadigas, M. ReaxFF Molecular Dynamics Simulations of Large Gold Nanocrystals. *J. Chem. Theory Comput.* (2022) 18, 4, 2521–2529.
31. Xia, Y.; Xiong, Y.; Lim, B.; Skrabalak, S. E. Shape-Controlled Synthesis of Metal Nanocrystals: Simple Chemistry Meets Complex Physics? *Angew. Chem., Int. Ed.* 2009, 48, 60–103.
32. Van Duin, A. C.; Dasgupta, S.; Lorant, F.; Goddard, W. A. ReaxFF: a reactive force field for hydrocarbons. *J. Phys. Chem. A* **2001**, 105, 9396-9409.
33. Chenoweth, K.; Van Duin, A. C.; Goddard, W. A. ReaxFF reactive force field for molecular dynamics simulations of hydrocarbon oxidation. *J. Phys. Chem. A* **2008**, 112, 1040-1053.
34. Mortier, W. J.; Ghosh, S. K.; Shankar, S. Electronegativity-equalization method for the calculation of atomic charges in molecules. *J. Am. Chem. Soc.* **1986**, 108, 4315-4320.
35. Janssens, G. O.; Baekelandt, B. G.; Toufar, H.; Mortier, W. J.; Schoonheydt, R. A. Comparison of cluster and infinite crystal calculations on zeolites with the electronegativity equalization method (EEM). *J. Phys. Chem.* **1995**, 99, 3251-3258.
36. Plimpton S., Fast Parallel Algorithms for Short-Range Molecular Dynamics. *J. Comp. Phys.* **1995**, 117, 1-19.
37. Aktulga, H. M.; Fogarty, J. C.; Pandit, S. A.; Grama, A. Y. Parallel reactive molecular dynamics: Numerical methods and algorithmic techniques. *Parallel Computing* **2012**, 38, 245-259.
38. Djebaili, T.; Richardi, J.; Abel, S.; Marchi, M. Atomistic simulations of the surface coverage of large gold nanocrystals. *J. Phys. Chem. C* 2013, 117, 17791–17800.
39. Djebaili, T.; Richardi, J.; Abel, S.; Marchi, M. Atomistic Simulations of Self-Assembled Monolayers on Octahedral and Cubic Gold Nanocrystals. *J. Phys. Chem. C* 2015, 119, 21146–21154.

ReaxFF Simulations of Self-Assembled Monolayers On Silver Surfaces and Nanocrystals

A. Lahouari,¹ J.-P. Piquemal,¹ J. Richardi^{1*}

1 Sorbonne Université, Laboratoire de Chimie Théorique, UMR 7616 CNRS, 75005
Paris, France

Supporting Information,

1. SAMmaker

The tool SAMmaker generates the positions of the metallic atoms and the ligands for a 33 and 77 SAMs. First, this tool calculates the positions of the metallic atoms of an fcc slab with its highest layers corresponding to the (111) plane. The lines of the metallic atoms building up the (111) plane points into the x direction as shown in the following figure S11. The user can then define the positions of the ligands for the first lines in the x direction. The headgroups of the ligands for a 77 SAM are colored in yellow in the following figure. These ligands are then repeated in the y direction taking into account a possible shift in the x direction. The user can choose the length of the alkyl chain and also specify the restructured conformation.

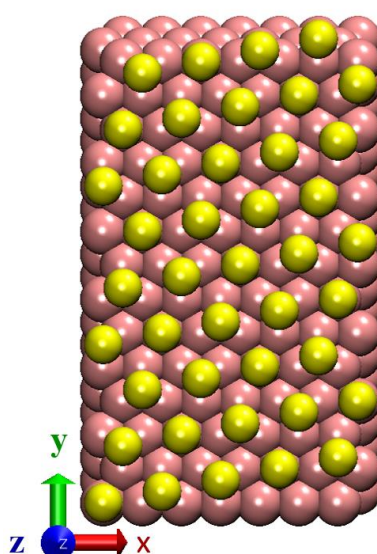


Figure S1: Ag (111) layer with the initial positions of the sulfur atoms in a 77 SAMs of thiolates.

2. SamFinder

In order to determine which ligands, belong to a self-assembled monolayer characterized as 33 or 77 we start as follows. First, a head group atom is picked up by accident. All surrounding head groups at a distance d_{SAM} within a precision of 10% are determined, where d_{SAM} is the distance usually observed for the investigated SAM (e.g. 5.0 Å for 33 and 4.39 Å for 77). Then, the distances between these surrounding atoms are calculated. Whenever one of the surrounding head groups has two neighbors at a distance d_{SAM} within a precision of 10%, it is counted as a new member of the SAM. In the following, new SAM members are chosen as centers and the procedure described above is reiterated. This percolation procedure stops when no newer neighboring atoms belonging to the SAM can be found. It is then restarted with a new

head group belonging to no SAM previously found and chosen by accident. This procedure continues until all head groups have been investigated.

3. Entropy

The free energy of a ligand in a SAM related to entropy can be obtained from equation:

$$F = -kT \ln q_t$$

where q_t is the partition function of translation for the ligand with mass m defined as

$$q_t = \frac{V}{h^3} \sqrt{2\pi mkT}$$

V is the volume in which the ligand can move for the SAM.

The difference in free energy between both SAMs can then be calculated from

$$\Delta F = -kT \ln (V_{77}/V_{33})$$

Using the relation $S = -(\partial F/\partial T)$, it can be seen this ΔF is directly related to the entropy.

It is now assumed that the ligand movement, perpendicular to the metallic surface, does not depend on the type of SAM, but on the metal-ligand interaction. Then the ratio of volumes can be approximated by $V_{77}/V_{33} \simeq S_{77}/S_{33}$ where S_{77} and S_{33} are the surface per ligand for both SAMs. It can be calculated for the 33 and 77 SAMs as 20.37 \AA^2 and 15.84 \AA^2 . This gives at 300 K for the free energy difference 0.149 kcal/mol which shows that the 33 SAM is entropically favored.

ReaxFF Simulations of Self-Assembled Monolayers On Silver Surfaces and Nanocrystals

A. Lahouari,¹ J.-P. Piquemal,¹ J. Richardi^{1*}

1 Sorbonne Université, Laboratoire de Chimie Théorique, UMR 7616 CNRS, 75005
Paris, France

Supporting Information, Figures

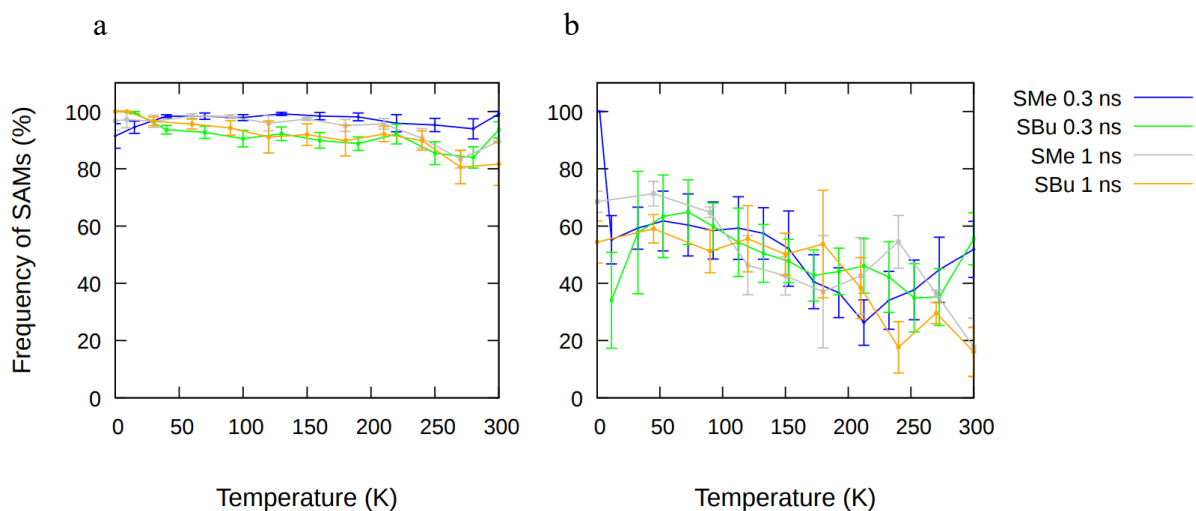


Figure S1: Frequencies of 77 (a) and 33 (b) SAMs of methane and butane thiolates on Ag(111) surface for an equilibration of 0.3 and 1 ns.

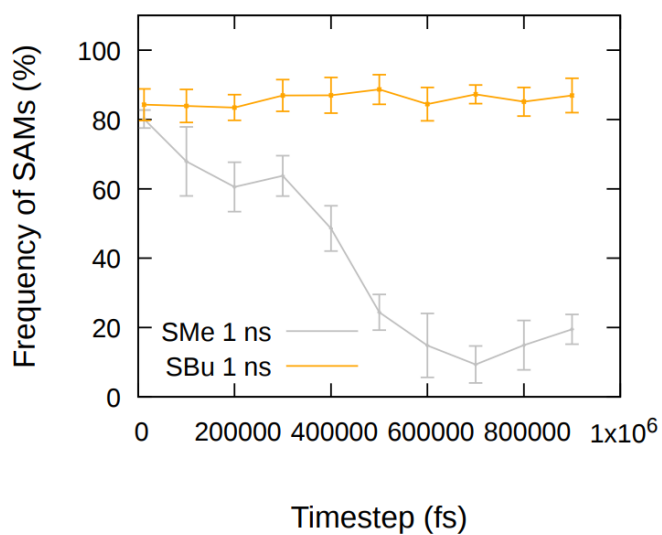


Figure S2: Frequencies of 77 SAMs of methane and butane thiolates on Ag (111) surface continuing the run after the equilibration of 3 ns for 1 ns.

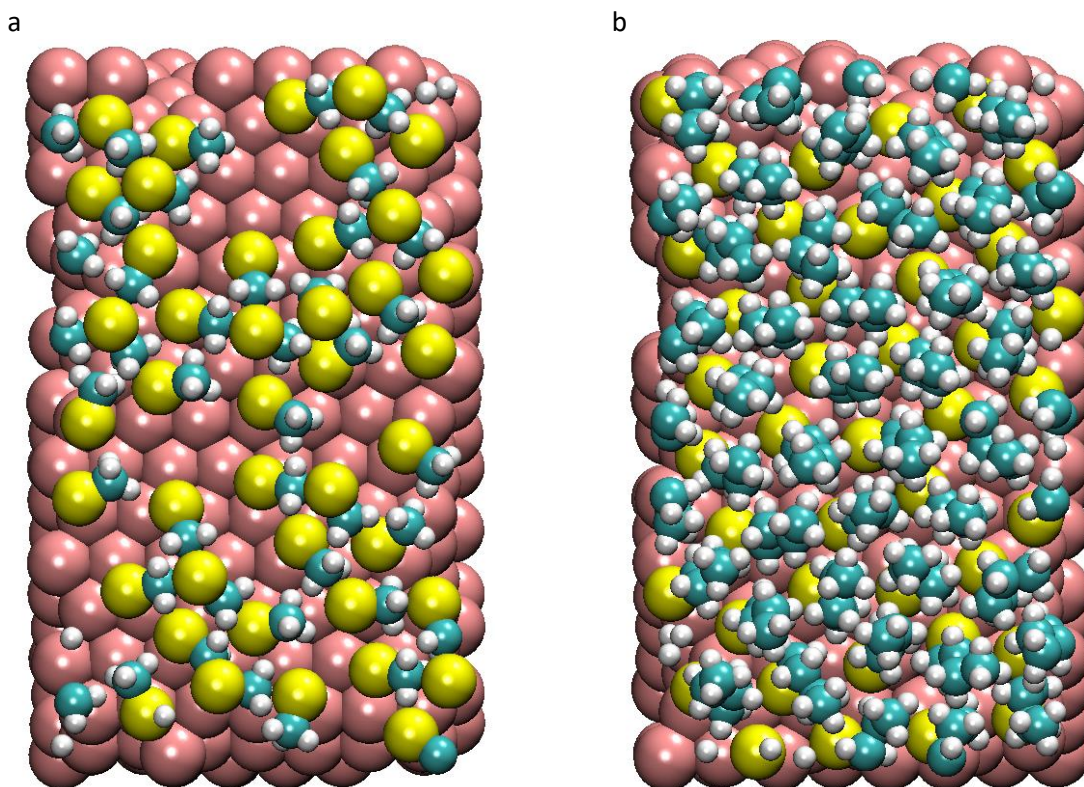


Figure S3: Snapshot of both the methane (a) and butane (b) thiolates SAMs on Ag(111) surface after 4 ns.

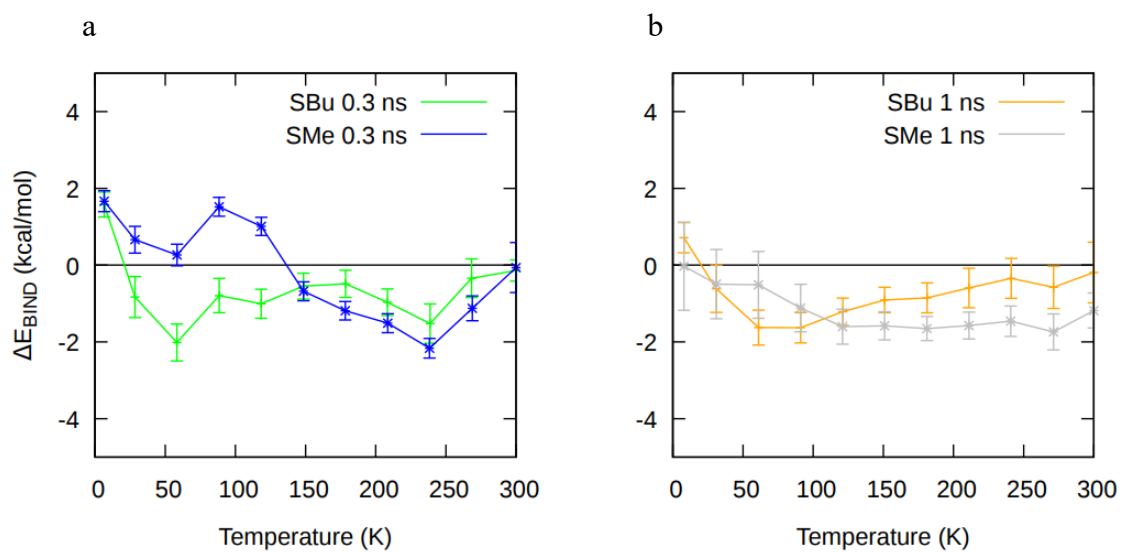


Figure S4: Difference of binding energies between the 77 and the 33 SAMs as a function of the temperature for both butane and methane thiolates on the Ag (111) surface. Simulation length: (a) 0.3 ns and (b) 1 ns.

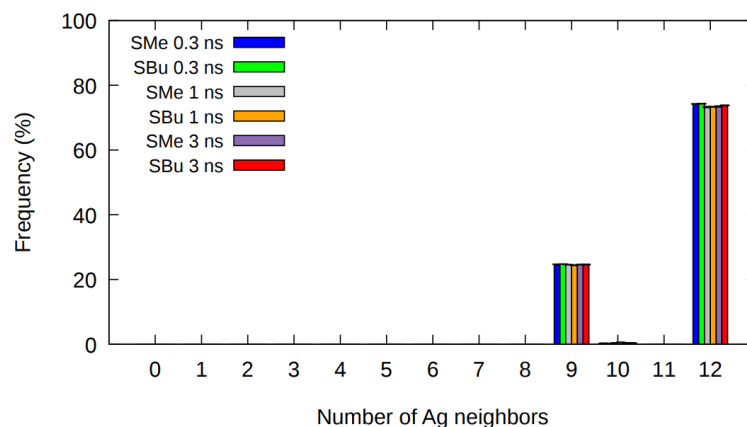


Figure S5: Frequencies of atoms as a function of the number of Ag neighbors for an Ag (111) surface with a SAM composed of methane or butane thiolates at different simulation length from 0.3 ns to 3 ns.

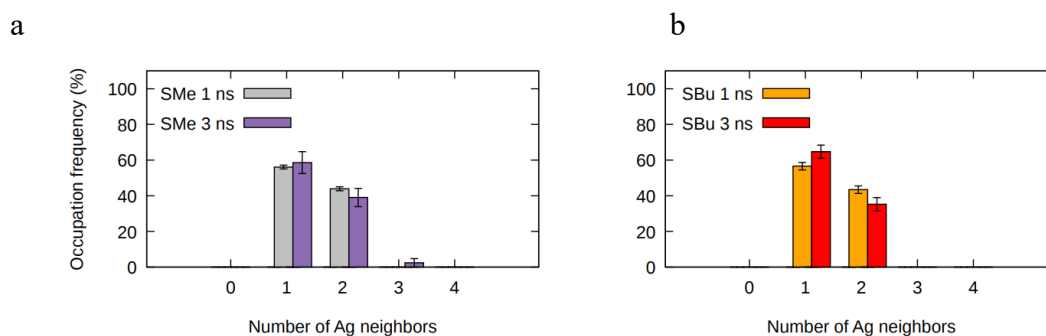


Figure S6: Occupation frequencies of adsorption sites on the facet for both (a) methane and (b) butane thiolates on Ag (111) surface at different simulation lengths, where respectively 1, 2 and 3 Ag neighbors correspond to on-top, bridge and hollow sites.

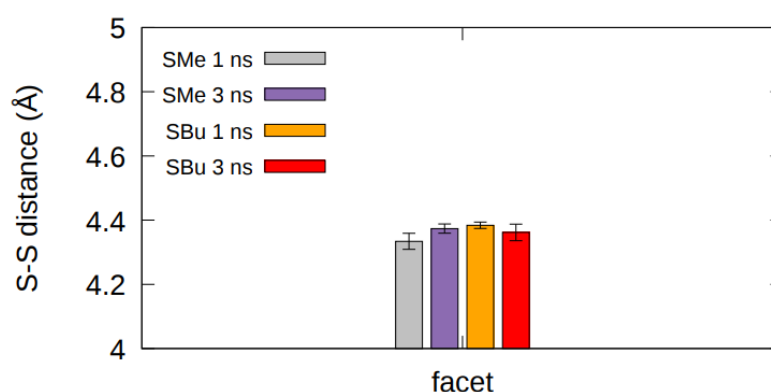


Figure S7: Average distance between sulfur atoms neighbors of methane and butane thiolates on a 77 SAM at different simulation lengths 1 ns and 3 ns. Result at the end of the equilibration at 300 K.

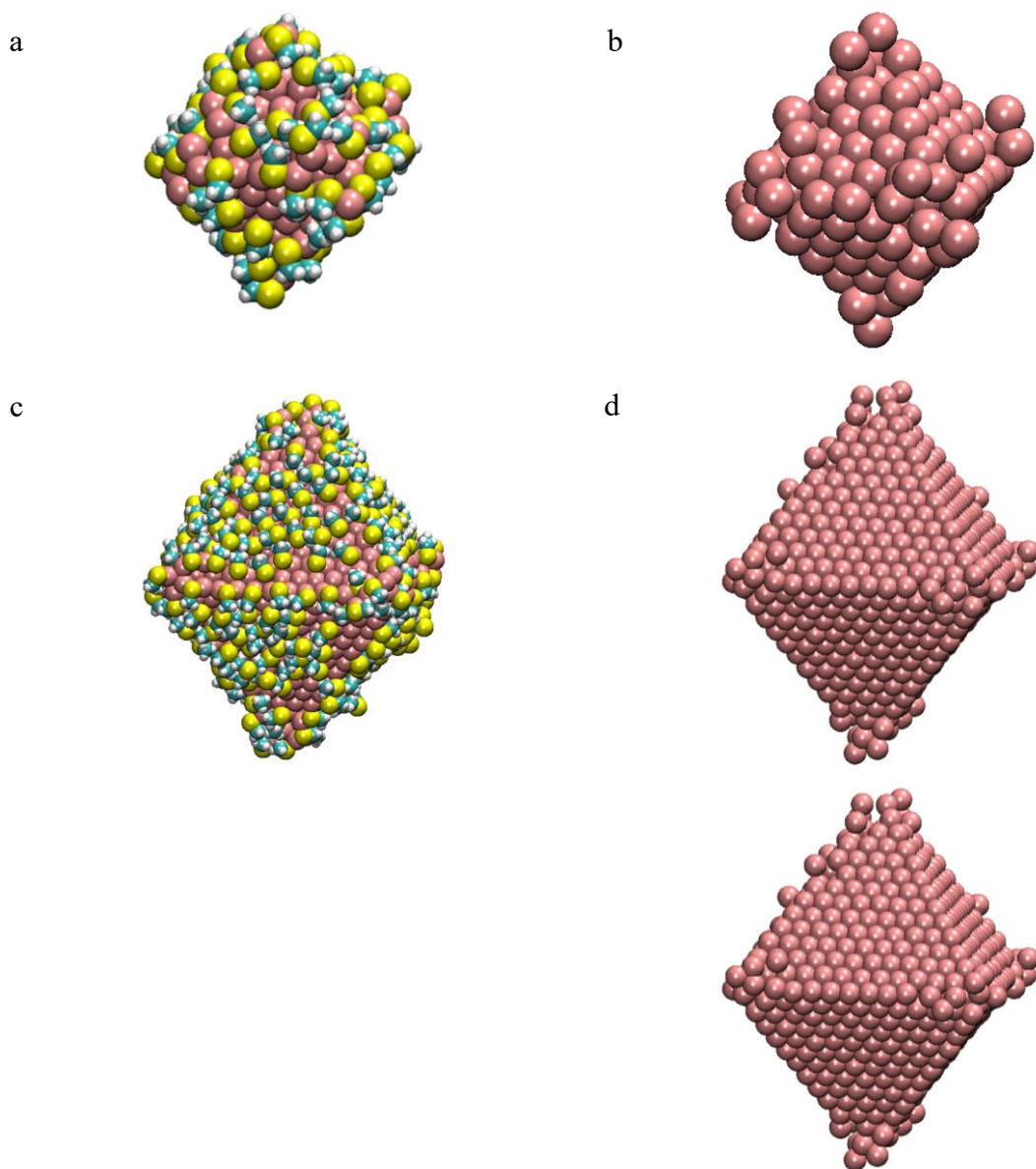


Figure S8: Snapshots of the simulation of methane thiolate covered silver nanoparticles of 2 nm (a) and 4 nm (c) at the end of the convergence step for 1 ns at 300 K. The ligands are removed to show any reconstruction of the metallic core on b and d snapshots.

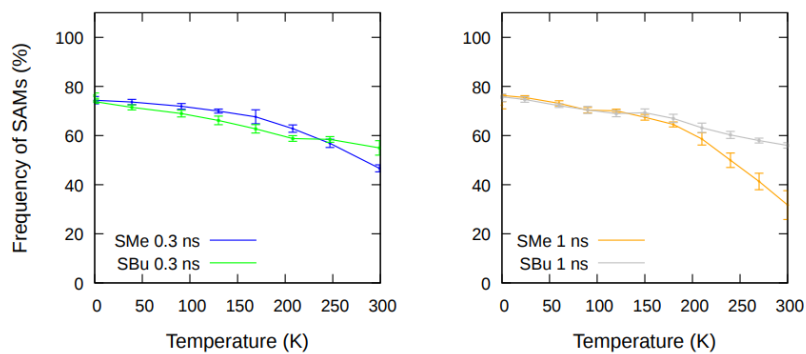


Figure S9: Frequencies of 77 SAM for both methane and butane thiolates SAMs on a 4 nm Ag (111) NP for different for 0.3 ns, 1 ns and 3 ns simulation length during the equilibration step.

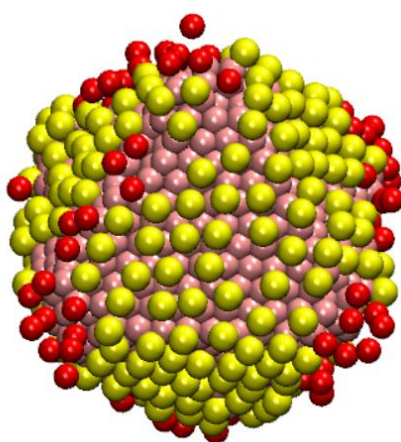


Figure S10: Snapshots of the simulation of a 77 butane thiolate SAMs on Ag (111) nanoparticles of 4 nm at the end of the convergence step for 1 ns at 300 K. Atoms belonging to the SAM are coloured in red.

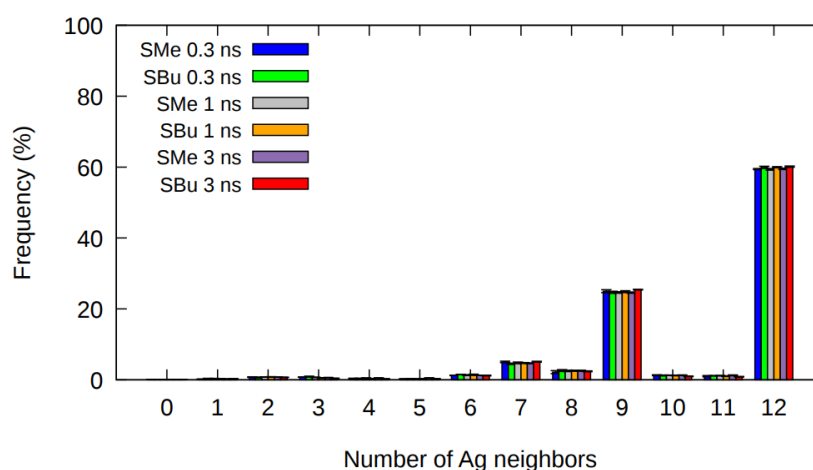


Figure S11: Frequencies of silver atoms as a function of their number of neighbours for 4 nm for methane and butane thiolate at different equilibration times from 0.3 ns to 3 ns. Property taken at the end of the convergence at 300K.

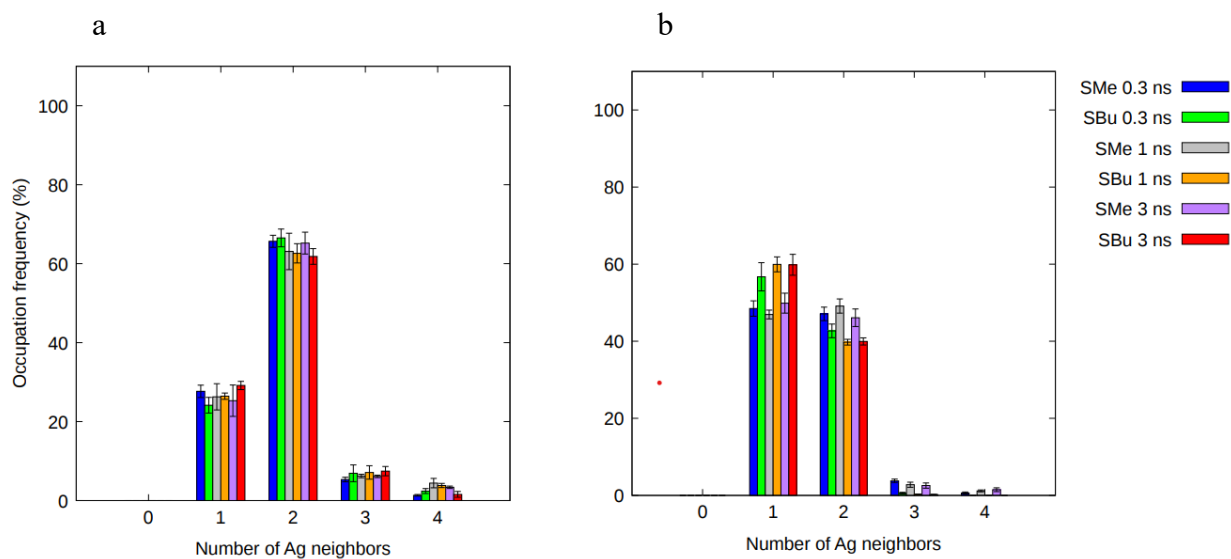


Figure S12: Occupation frequencies of adsorption sites on the (a) edges and (b) facets for both methane and butane thiolates on an Ag (111) nanoparticle of 4 nm, where respectively 1, 2 and 3 Ag neighbours correspond to top, bridge and hollow sites. Results for equilibration times 0.3, 1 and 3 ns at the end of the convergence at 300 K.

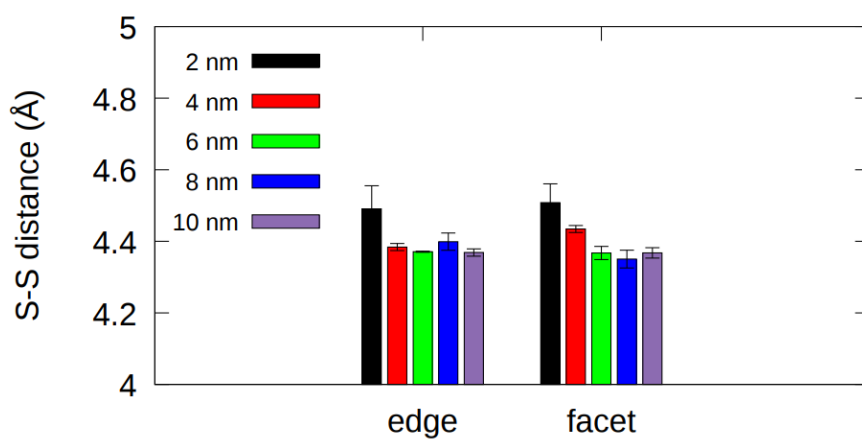


Figure S13: Average S-S distance between first neighbors on the edges and facets of silver NPs from 2 to 10 nm for methane thiolates at the end of convergence at 300K for an equilibration length of 1 ns.

ReaxFF Simulations of Self-Assembled Monolayers On Silver Surfaces and Nanocrystals

A. Lahouari,¹ J.-P. Piquemal,¹ J. Richardi^{1*}

1 Sorbonne Université, Laboratoire de Chimie Théorique, UMR 7616 CNRS, 75005
Paris, France

Supporting Informations

Table S1. Average distances between neighboring S head groups. The results are given for different silver nanocrystal diameters and both methane and butane thiolate. The values on the vertex, edges and facets are shown.

2 nm / SMe	
vertex	4.48 ± 0.05
edge	4.49 ± 0.06
facet	4.51 ± 0.05
4 nm / SMe	
vertex	4.49 ± 0.08
edge	4.38 ± 0.01
facet	4.43 ± 0.01
6 nm / SMe	
vertex	4.44 ± 0.05
edge	4.37 ± 0.00
facet	4.37 ± 0.02
8 nm / SMe	
vertex	4.47 ± 0.04
edge	4.40 ± 0.02
facet	4.35 ± 0.02
10 nm / SMe	
vertex	4.40 ± 0.01
edge	4.37 ± 0.01
facet	4.37 ± 0.01
2 nm / SBu	
total	4.44 ± 0.01
vertex	4.39 ± 0.01
edge	4.39 ± 0.01
4 nm / SBu	
total	4.43 ± 0.01
vertex	4.37 ± 0.04
edge	4.34 ± 0.02
6 nm / SBu	
total	4.35 ± 0.00
vertex	4.34 ± 0.07
edge	4.22 ± 0.01
8 nm / SBu	
total	4.31 ± 0.00
vertex	4.32 ± 0.06
edge	4.23 ± 0.00
10 nm / SBu	
total	4.29 ± 0.01
vertex	4.41 ± 0.10
edge	4.26 ± 0.01

Table S2. Relative frequencies of the S head group as a function of their adsorption position for silver nanocrystals with methane and butane thiolate.

2 nm / SMe		
vertex	edge	facet
15.57 ± 0.87	62.23 ± 2.51	22.23 ± 3.38
4 nm / SMe		
vertex	edge	facet
1.77 ± 0.32	28.70 ± 0.29	69.53 ± 0.58
6 nm / SMe		
vertex	edge	facet
2.37 ± 0.15	29.03 ± 0.37	68.60 ± 0.40
8 nm / SMe		
vertex	edge	facet

	1.37 ± 0.03	22.63 ± 0.37	76.00 ± 0.35
10 nm / SMe			
vertex		edge	facet
	0.87 ± 0.03	18.27 ± 0.26	80.90 ± 0.29
2 nm / SBu			
vertex		edge	facet
	16.99 ± 0.63	65.77 ± 1.06	17.26 ± 0.88
4 nm / SBu			
vertex		edge	facet
	4.93 ± 0.23	39.37 ± 1.13	55.67 ± 0.96
6 nm / SBu			
vertex		edge	facet
	2.20 ± 0.06	26.27 ± 0.44	71.57 ± 0.49
8 nm / SBu			
vertex		edge	facet
	1.13 ± 0.09	21.53 ± 0.33	77.33 ± 0.41
10 nm / SBu			
vertex		edge	facet
	0.67 ± 0.07	18.23 ± 0.18	81.07 ± 0.23

Table S3. Frequencies of silver atoms with a given number of neighbors for silver nanocrystals with methane and butane thiolate. First line denoted by "total" gives the absolute number. All other values are given in %.

2 nm / SMe										
Neighbors	0	1	2	3	4	5	6			
Frequency	0.13 ± 0.13	1.63 ± 0.55	2.77 ± 0.61	3.13 ± 0.61	1.47 ± 0.30	1.17 ± 0.26	5.70 ± 0.50			
Neighbors	7	8	9	10	11	12				
Frequency	13.90 ± 0.23	6.13 ± 0.93	25.07 ± 0.78	3.33 ± 0.32	7.43 ± 0.47	25.57 ± 0.69				
4 nm / SMe										
Neighbors	0	1	2	3	4	5	6			
Frequency	0.03 ± 0.03	0.13 ± 0.03	0.40 ± 0.06	0.37 ± 0.03	0.17 ± 0.03	0.20 ± 0.06	0.90 ± 0.10			
Neighbors	7	8	9	10	11	12				
Frequency	5.90 ± 0.12	1.40 ± 0.06	26.33 ± 0.13	1.13 ± 0.15	0.50 ± 0.06	60.23 ± 0.09				
6 nm / SMe										
Neighbors	0	1	2	3	4	5	6			
Frequency	0.00 ± 0.00	0.03 ± 0.03	0.17 ± 0.03	0.23 ± 0.03	0.13 ± 0.03	0.10 ± 0.00	0.33 ± 0.03			
Neighbors	7	8	9	10	11	12				
Frequency	2.83 ± 0.03	0.67 ± 0.03	20.63 ± 0.09	0.83 ± 0.07	0.50 ± 0.00	71.53 ± 0.07				
8 nm / SMe										
Neighbors	0	1	2	3	4	5	6			
Frequency	0.00 ± 0.00	0.00 ± 0.00	0.10 ± 0.00	0.13 ± 0.03	0.10 ± 0.00	0.03 ± 0.03	0.20 ± 0.00			
Neighbors	7	8	9	10	11	12				
Frequency	1.60 ± 0.00	0.50 ± 0.00	16.60 ± 0.00	0.70 ± 0.00	0.23 ± 0.03	77.73 ± 0.07				
10 nm / SMe										
Neighbors	0	1	2	3	4	5	6			
Frequency	0.00 ± 0.00	0.00 ± 0.00	0.00 ± 0.00	0.10 ± 0.00	0.07 ± 0.03	0.00 ± 0.00	0.10 ± 0.00			
Neighbors	7	8	9	10	11	12				
Frequency	1.10 ± 0.00	0.30 ± 0.00	13.97 ± 0.03	0.53 ± 0.03	0.17 ± 0.03	81.60 ± 0.06				
2 nm / SBu										
Neighbors	0	1	2	3	4	5	6			
Frequency	0.44 ± 0.11	2.14 ± 0.41	4.59 ± 0.43	3.92 ± 0.20	1.69 ± 0.17	1.78 ± 0.29	6.47 ± 0.63			
Neighbors	7	8	9	10	11	12				
Frequency	10.51 ± 0.79	8.37 ± 0.54	21.60 ± 0.44	3.70 ± 0.48	8.47 ± 0.35	23.99 ± 0.39				
4 nm / SBu										
Neighbors	0	1	2	3	4	5	6			
Frequency	0.10 ± 0.00	0.30 ± 0.00	0.80 ± 0.10	0.53 ± 0.09	0.37 ± 0.03	0.30 ± 0.06	1.43 ± 0.18			
Neighbors	7	8	9	10	11	12				
Frequency	4.73 ± 0.13	2.57 ± 0.15	24.87 ± 0.27	1.23 ± 0.09	1.03 ± 0.12	59.97 ± 0.17				
6 nm / SBu										
Neighbors	0	1	2	3	4	5	6			
Frequency	0.00 ± 0.00	0.10 ± 0.00	0.20 ± 0.00	0.13 ± 0.03	0.03 ± 0.03	0.10 ± 0.00	0.40 ± 0.00			
Neighbors	7	8	9	10	11	12				
Frequency	2.80 ± 0.00	0.73 ± 0.03	20.50 ± 0.06	0.83 ± 0.03	0.50 ± 0.06	71.73 ± 0.09				
8 nm / SBu										
Neighbors	0	1	2	3	4	5	6			
Frequency	0.00 ± 0.00	0.10 ± 0.00	0.17 ± 0.03	0.10 ± 0.00	0.03 ± 0.03	0.03 ± 0.03	0.27 ± 0.03			
Neighbors	7	8	9	10	11	12				
Frequency	1.50 ± 0.00	0.60 ± 0.00	16.47 ± 0.03	0.63 ± 0.03	0.23 ± 0.03	78.03 ± 0.07				
10 nm / SBu										
Neighbors	0	1	2	3	4	5	6			

Frequency 0.00 ± 0.00 0.00 ± 0.00 0.10 ± 0.00 0.10 ± 0.00 0.03 ± 0.03 0.00 ± 0.00 0.17 ± 0.03
 Neighbors 7 8 9 10 11 12
 Frequency 1.03 ± 0.03 0.40 ± 0.00 13.87 ± 0.03 0.50 ± 0.00 0.20 ± 0.00 81.87 ± 0.03

Table S4. Frequencies of the S atoms in contact with a given number of silver atoms for silver nanocrystals with methane and butane thiolate.

2 nm / SMe					
Neighbors	0	1	2	3	4
vertex	0.00 ± 0.00	25.71 ± 4.82	71.53 ± 2.76	2.76 ± 2.76	0.00 ± 0.00
edge	0.00 ± 0.00	27.16 ± 1.49	64.28 ± 2.56	6.64 ± 3.49	1.93 ± 1.27
facet	0.00 ± 0.00	50.74 ± 17.60	46.69 ± 3.02	2.57 ± 1.71	0.00 ± 0.00
centre	0.00 ± 0.00	0.00 ± 0.00	0.00 ± 0.00	0.00 ± 0.00	0.00 ± 0.00
4 nm / SMe					
Neighbors	0	1	2	3	4
vertex	0.00 ± 0.00	32.95 ± 4.05	30.64 ± 5.20	28.90 ± 9.83	7.51 ± 4.05
edge	0.00 ± 0.00	28.65 ± 0.70	68.12 ± 1.91	1.50 ± 0.10	1.74 ± 0.52
facet	0.00 ± 0.00	52.13 ± 2.53	46.04 ± 2.29	1.15 ± 0.22	0.68 ± 0.22
centre	0.00 ± 0.00	0.00 ± 0.00	0.00 ± 0.00	0.00 ± 0.00	0.00 ± 0.00
6 nm / SMe					
Neighbors	0	1	2	3	4
vertex	0.00 ± 0.00	29.54 ± 2.53	54.85 ± 6.33	7.17 ± 5.06	8.44 ± 4.22
edge	0.00 ± 0.00	25.84 ± 1.72	69.34 ± 2.58	3.00 ± 0.96	1.83 ± 0.41
facet	0.00 ± 0.00	61.41 ± 1.02	38.29 ± 1.53	0.19 ± 0.04	0.10 ± 0.10
centre	0.00 ± 0.00	0.00 ± 0.00	0.00 ± 0.00	0.00 ± 0.00	0.00 ± 0.00
8 nm / SMe					
Neighbors	0	1	2	3	4
vertex	0.00 ± 0.00	23.74 ± 2.16	64.75 ± 0.00	9.35 ± 2.16	2.16 ± 2.16
edge	0.00 ± 0.00	27.40 ± 1.99	67.30 ± 2.12	3.23 ± 0.40	2.08 ± 0.66
facet	0.00 ± 0.00	58.74 ± 0.53	41.13 ± 0.12	0.13 ± 0.08	0.00 ± 0.00
centre	0.00 ± 0.00	0.00 ± 0.00	0.00 ± 0.00	0.00 ± 0.00	0.00 ± 0.00
10 nm / SMe					
Neighbors	0	1	2	3	4
vertex	0.00 ± 0.00	20.24 ± 3.57	67.86 ± 10.71	11.90 ± 0.00	0.00 ± 0.00
edge	0.00 ± 0.00	28.42 ± 0.66	67.38 ± 1.31	2.19 ± 0.55	2.02 ± 0.16
facet	0.00 ± 0.00	59.77 ± 0.64	39.95 ± 0.19	0.28 ± 0.11	0.00 ± 0.00
centre	0.00 ± 0.00	0.00 ± 0.00	0.00 ± 0.00	0.00 ± 0.00	0.00 ± 0.00
2 nm / SBu					
Neighbors	0	1	2	3	4
vertex	0.00 ± 0.00	12.51 ± 3.19	70.32 ± 4.78	15.87 ± 2.89	1.30 ± 0.71
edge	0.00 ± 0.00	13.98 ± 1.67	65.36 ± 1.78	15.82 ± 1.78	4.85 ± 0.76
facet	0.00 ± 0.00	47.19 ± 3.65	52.58 ± 5.68	0.23 ± 0.23	0.00 ± 0.00
centre	0.00 ± 0.00	0.00 ± 0.00	0.00 ± 0.00	0.00 ± 0.00	0.00 ± 0.00
4 nm / SBu					
Neighbors	0	1	2	3	4
vertex	0.00 ± 0.00	15.71 ± 3.47	76.12 ± 3.06	6.12 ± 0.00	2.04 ± 2.04
edge	0.00 ± 0.00	26.44 ± 0.79	62.62 ± 2.44	7.12 ± 1.70	3.81 ± 0.53
facet	0.00 ± 0.00	59.94 ± 1.94	39.75 ± 0.75	0.31 ± 0.05	0.00 ± 0.00
centre	0.00 ± 0.00	0.00 ± 0.00	0.00 ± 0.00	0.00 ± 0.00	0.00 ± 0.00
6 nm / SBu					
Neighbors	0	1	2	3	4
vertex	0.00 ± 0.00	0.00 ± 0.00	0.00 ± 0.00	3.18 ± 1.36	96.82 ± 5.45
edge	0.00 ± 0.00	23.37 ± 0.69	56.69 ± 1.03	6.98 ± 0.57	12.96 ± 1.33
facet	0.00 ± 0.00	64.09 ± 1.91	35.67 ± 1.50	0.24 ± 0.13	0.00 ± 0.00
centre	0.00 ± 0.00	0.00 ± 0.00	0.00 ± 0.00	0.00 ± 0.00	0.00 ± 0.00
8 nm / SBu					
Neighbors	0	1	2	3	4
vertex	0.00 ± 0.00	0.00 ± 0.00	0.00 ± 0.00	0.00 ± 0.00	100.00 ± 7.96
edge	0.00 ± 0.00	10.37 ± 0.33	24.19 ± 0.47	3.26 ± 0.93	62.19 ± 1.07
facet	0.00 ± 0.00	47.03 ± 0.66	27.91 ± 0.84	0.99 ± 0.16	24.07 ± 0.37
centre	0.00 ± 0.00	0.00 ± 0.00	0.00 ± 0.00	0.00 ± 0.00	0.00 ± 0.00
10 nm / SBu					
Neighbors	0	1	2	3	4

vertex	0.00 ± 0.00	0.00 ± 0.00	0.00 ± 0.00	0.00 ± 0.00	100.00 ±10.45
edge	0.00 ± 0.00	2.19 ± 0.33	6.01 ± 0.93	2.73 ± 0.33	89.07 ± 0.33
facet	0.00 ± 0.00	24.49 ± 0.27	15.04 ± 0.18	1.48 ± 0.00	59.00 ± 0.37
centre	0.00 ± 0.00	0.00 ± 0.00	0.00 ± 0.00	0.00 ± 0.00	0.00 ± 0.00